RESEARCH PAPER

Metformin-copper-dendrimer: a new nanotherapeutic agent for diabetic breast cancer studies

Kimia Esmaeilzadeh[1], Farinaz Khalatbari[2], Sepehr Ashrafi [3], Mohammad Seyedhamzeh[2], Seyed Esmaiel Sadat Ebrahimi[2], Mehdi Shafiee Ardestani [2, 4*]*

[1]*Department of Medical Nanotechnology, School of Medicine, Zanjan University of Medical Sciences, Zanjan, Iran*
[2]*Department of Radio Pharmacy, Faculty of Pharmacy, Tehran University of Medical Sciences, Tehran, Iran*
[3] *Ramsar Campus, Mazandaran University of Medical Sciences, Ramsar, Iran*
[4] *Research Center for Nuclear Medicine, Shariati Hospital, North Kargar Ave. 1411713135, Tehran, Iran*

ABSTRACT

Objective(s): Design and test a metformin–copper–anionic linear dendrimer theranostic complex for breast cancer.

Materials and Methods: Dendrimer–copper complex was synthesized and attached to the metformin. The physicochemical characterizations comprised FTIR, DLS, TEM and XPS. MTT assay and Annexin V/propidium iodide flow cytometry were used to evaluate the cytotoxicity and apoptosis in 4T1 breast cancer cells. Nanocomplex was labeled with technetium-99m for SPECT imaging and biodistribution studies in tumor bearing BALB/c mice.

Results: The reported hydrodynamic diameter was 26 nm for the dendrimer, 90 nm for the Cu incorporated dendrimer and 95 nm for the metformin conjugated dendrimer and final zeta potential was found to be around +3 mV. The average particle diameter was determined using TEM, which was 36.94 ± 6.33 nm. The viability of 4T1 cells was lower in the concentration of the metformin-containing nanocomplex than in the concentration of the copper–dendrimer complex. Imaging and biodistribution experiments showed that the radiolabeled nanocomplex localized on tumor.

Conclusion: Metformin–copper–dendrimer system exhibited in vitro antitumor activity and tumor localization in mice, suggesting its potential in the further research as a theranostic agent against breast cancer.

Keywords: *Breast cancer; Copper; Dendrimer; Metformin; Nanotheranostics; SPECT imaging*

How to cite this article

Esmaeilzadeh K, Khalatbari F, Ashrafi S, Seyedhamzeh M, Sadat Ebrahimi SE, Shafiee Ardestani M. Metformin-copper-dendrimer: a new nanotherapeutic agent for diabetic breast cancer studies. Nanomed J. 2027; 14: 1-. DOI: 10.22038/nmj.2026.81697.2032

Corrected Proof

INTRODUCTION

In modern medicine, cancer represents a significant and complex challenge that affects a large number of individuals worldwide [1]. Conventional cancer therapies, such as radiation therapy and chemotherapy, have limited effectiveness and can lead to severe side effects. The discovery of novel cell death mechanisms has opened new avenues for innovative cancer treatments in the rapidly advancing field of oncology [2]. A recent breakthrough in this area is cuproptosis, a unique form of cellular death induced by the accumulation of copper within cells. Cuproptosis differs from apoptosis, necrosis, and ferroptosis, as it does not depend on the caspase pathway, reactive oxygen species (ROS), or lipid peroxidation [3]. Instead, it involves the direct binding of copper to components of the tricarboxylic acid (TCA) cycle, resulting in the aggregation and inactivation of iron-sulfur cluster proteins, which disrupts cellular metabolism and ultimately triggers cell death. This novel mechanism offers a distinct opportunity to selectively target cancer cells, which often exhibit disrupted copper homeostasis [4]**.** Cuproptosis is characterized by the toxic accumulation of copper within cells, leading to mitochondrial dysfunction and ultimately resulting in cell death. This process is distinct from other recognized cell death pathways, primarily involving the selective targeting and disruption of the tricarboxylic acid (TCA) cycle within the mitochondria. Copper interacts directly with lipoylated components of the TCA cycle, particularly dihydrolipoamide S-acetyltransferase (DLAT), a key enzyme in the pyruvate dehydrogenase complex. This interaction leads to the accumulation of lipoylated proteins and the destabilization of iron-sulfur cluster proteins, essential for various metabolic processes. Ultimately, this disrupts cellular metabolism and triggers cell death. The identification of cuproptosis has significant implications for cancer therapy, as several types of cancer exhibit abnormal copper metabolism, with higher levels of copper in

* *Corresponding author:* Mehdi Shafiee Ardestani, Associate Professor, Department of Radio Pharmacy, Faculty of Pharmacy, Tehran University of Medical Sciences, Tehran, Iran. Phone: +98 9128267629, Email: *Shafieeardestani@gmail.com*. Sepehr Ashrafi, Ramsar Campus, Mazandaran University of Medical Sciences, Ramsar, Iran. Phone: +98 9129513319, Email: *sepehrpharmacy@gmail.com*.

Note. This manuscript was submitted on August 05, 2024; approved on October 29, 2024.

© 2027. This work is openly licensed via CC BY 4.0. This is an Open Access article distributed under the terms of the Creative Commons Attribution License (https://creativecommons.org/licenses), which permits unrestricted use, distribution, and reproduction in any medium, provided the original work is properly cited.

malignant cells compared to healthy tissues [5]. The difference in copper metabolism between normal and cancer cells enables the targeted destruction of tumor cells through the induction of cuproptosis. Researchers are exploring small compounds capable of transporting copper ions across cell membranes [6]. These molecules are being studied for their potential to elevate copper levels in cancer cells, triggering cuproptosis. Preclinical studies have demonstrated that combining drugs such as disulfiram, commonly used to treat alcohol dependence, with copper shows a promising anticancer effect. By modulating the expression of proteins involved in copper transport and storage, such as CTR1 (copper transporter 1), ATP7A, and ATP7B, it is possible to alter intracellular copper levels and selectively induce cuproptosis in cancer cells [7–9].

Epidemiological studies indicate that approximately 16% of individuals diagnosed with breast cancer also have diabetes. Research suggests that having diabetes before the onset of breast cancer is an independent and significant factor that increases the likelihood of disease development and progression. A study conducted on Asian women found no correlation between a previous diagnosis of diabetes and an increased risk of developing breast cancer [10]. Medications used in breast cancer treatment can elevate the risk of patients developing diabetes. A challenge in imaging with contrast agents in these patients is the need for fasting. For example, obese diabetic patients generally require higher doses of FDG to obtain satisfactory images [11]. However, the Commission on Radiological Protection restricts the dosages that can be administered. These limitations can be mitigated by extending the duration of data acquisition, though this results in longer scanning times and an increased risk of motion artifacts. Metformin, a widely studied medication, has been used in the treatment of both diabetes and breast cancer. The evaluation of the impact of preexisting diabetes on the occurrence and progression of breast cancer in clinical research primarily relies on cohort studies and meta-analyses. Data is collected after drug intervention for diabetes and breast cancer, and the varying effects of drug intervention can lead to conflicting results [11].

Metformin is a pharmacological agent used to treat diabetes by inhibiting glucose production in the liver and enhancing the body's response to insulin. The anticancer activity of metformin is mediated through both direct and indirect pathways [12]. The direct effects include inhibiting cancer cell growth, inducing programmed cell death, and reducing tumor stem-like cells. These effects are achieved by lowering the activity of mitochondrial respiratory Complex I and activating LKB1 and AMPK, which subsequently suppresses mTOR [13]. Metformin can also disrupt the function of hexokinase I and II and inhibit the activity of HER2 tyrosine kinase, particularly in breast cancer cells overexpressing HER2 [14]. Additionally, it can interfere with the signaling pathways associated with STAT3 [15]. Indirect benefits include improved insulin sensitivity and reduced inflammation, leading to lower circulating levels of insulin and IGF-1, which contribute to the prevention and treatment of cancer progression [16].

MATERIALS AND METHODS

High-quality analytical chemical reagents were used without further purification. Transmission electron microscopy (TEM) analyzed elemental characteristics and distribution. Dynamic light scattering (DLS) measurements were performed using the Malvern Nano-ZS device, while static light scattering (SLS) analysis was conducted with the Zetasizer ZSP apparatus. Sodium pertechnetate ($Na^{99}mTcO_4$) was produced using a $^{99}Mo/^{99}mTc$ generator with isotonic sodium chloride solution at pH 7.4. SPECT imaging was performed using a Siemens Dual-head γ-camera (E.cam). Quantitative gamma counting was done with an ORTEC Model 4001 M c-system well counter. Biodistribution studies were conducted on female BALB/c mice, aged six to seven weeks and weighing 23 to 27 grams, which were injected subcutaneously with 4T1 cells. The mice had free access to water and standard laboratory food. All experiments were repeated three times. The research adhered to the Animal Care and Use Committee guidelines of Tehran University of Medical Sciences.

Synthetic procedures

" A dendrimer was synthesized based on our previous research [17].To generate dendrimer-copper complex nanoparticles of uniform size, 0.35 mL of a 0.1 M copper sulfate ($CuSO_4$) solution was added to a test tube containing 3 mL of a dendrimer solution at a 10 mg/mL concentration. The two solutions were allowed to mix for approximately 5 minutes. Subsequently, 10 mL of a freshly prepared, chilled 0.04 M $NaBH_4$ solution was introduced into the mixture. The solution was stirred at a temperature range of 26–28°C. After approximately 18 hours, the mixture changed to a golden hue. The product was separated from the solution by centrifugation at 12,000 revolutions per minute (RPM) for 15 to 20 minutes, followed by extensive washing with ethanol and deionized water (16 times). A solution was prepared to conjugate metformin with the nanoparticle by dissolving 20 mg of the nanoparticle in a mixture of 4 mL of water and dimethylformamide. The solution was then supplemented with 0.02 mmol of EDC and 0.01 mmol of NHS and allowed to react for

Corrected Proof

30 minutes. After adjusting the pH of the solution to 9 using a buffer, 20 mg of metformin was added over 7 hours. Upon completion of the reaction, the purification process commenced.

ROS assay

MB and H_2O_2 solutions were enriched with samples containing dendrimer and dendrimer-Cu-metformin at a 0.3 mg/mL concentration. The reactions were carried out at a temperature of 37 °C. The level of reactive oxygen species (ROS) produced was determined by quantifying the breakdown of methylene blue (MB) at a wavelength of 650 nm following a 30-minute exposure to hydroxyl radicals (•OH) [18].

Ninhydrin Assay

A 500 µL aliquot of nanoparticle dispersion (containing 5 mg of nanoparticles) was centrifuged, ethanol was replaced with water, and sonication was performed to redisperse the nanoparticles. The sample was then combined with KCN, phenol, and ninhydrin reagents and subjected to heating in a water bath at 97 °C for 10 minutes. After cooling, the sample was transferred to a volumetric flask and diluted to 5 mL with 60% ethanol. A 200 µL aliquot was centrifuged, and the supernatant was analyzed using UV-Vis spectrophotometry, ensuring the optical density remained below 0.8 at 570 nm. The assay was calibrated with octylamine concentrations.

Toxicity assay

This method is a competitive mitochondrial metabolic assay that relies on reducing tetrazolium salt by the enzyme succinate dehydrogenase in living cells. In the procedure, 100 µL of culture medium containing 30,000 cells was placed in each well of a 96-well plate. After 24 hours of incubation, nanodrugs at 200 and 400 µg/mL concentrations were added and incubated for another 48 hours in a CO_2 incubator. Subsequently, 20 µL of MTT (5 mg/mL) was added to each well and incubated for 4 hours in the dark. The culture medium with MTT was then carefully removed, and 200 µL of acidified isopropanol was added to dissolve the purple formazan. After 15 minutes of incubation at room temperature, the optical density of each well was measured using an ELISA reader at 570 nm with a reference wavelength of 690 nm.

Flow Cytometry

To evaluate the cytotoxic effects of Metformin-Cu-Dendrimer, 4T1 cells were seeded into a 6-well plate and incubated under various conditions for 24 hours. The cells were treated with 0.25% trypsin, washed thrice with ice-cold PBS, and resuspended in 195 µL of binding buffer. A solution containing 10 µL of propidium iodide (PI) and 5 µL of Annexin V-FITC was added and incubated at room temperature for 20 minutes. Finally, the cells were analyzed using a flow cytometer.

Labeling

Radiochemical purity was assessed using Whatman No. 2 paper as the solid phase and two solvent systems: a 1:1 ratio of acetone to methanol and a saline solution as the mobile phase. A small volume (5 µL) of the labeled kit was applied 1 cm from the bottom of the strip, which was then placed in a chromatography tank. After the solvent front had traveled approximately 10 cm, the strip was dried and cut into 1-cm sections. The radioactivity in each section was measured using a gamma well counter.

When saline was used, $^{99m}TcO_2$ remained at the starting point, while the labeled conjugate and $^{99m}TcO_4^-$ migrated with the solvent front. In contrast, with acetone/methanol, $^{99m}TcO_2$ and the labeled conjugate remained stationary, while $^{99m}TcO_4^-$ migrated. Radiochemical purity is calculated by subtracting the sum of $^{99m}TcO_4^-$ and $^{99m}TcO_2$ from 100, or by dividing the activity in the initial 2 cm by the total activity to determine labeling efficiency. The studies indicated that the presence of water reduces yield and increases $^{99m}TcO_2$, prompting the formulation of the kit in a lyophilized state to mitigate the negative impact of water.

Injection of the labeled compound into mice and imaging with the SPECT technique

Mice were anesthetized with a ketamine/xylazine mixture and placed in a restrainer. Each mouse received an injection of 0.5 mL (approximately 1.4 mCi) of a labeled compound through the tail vein using an insulin syringe. Positioned on their backs, the mice underwent tissue uptake imaging at 90 minutes and whole-body imaging to assess post-injection clarity and contrast. Following radiopharmaceutical administration, additional imaging was performed at 120 minutes. Mice were euthanized painlessly while still under anesthesia at the 90-minute mark, under ethical guidelines. Target tissues (liver, kidneys, lungs, heart, brain, spleen, intestines, and bladder) were isolated, and their activity levels were measured using a dose calibrator. Organ weights were recorded, and activity levels were calculated as a percentage of total activity per gram of tissue, presented as mean ± standard deviation.

Corrected Proof

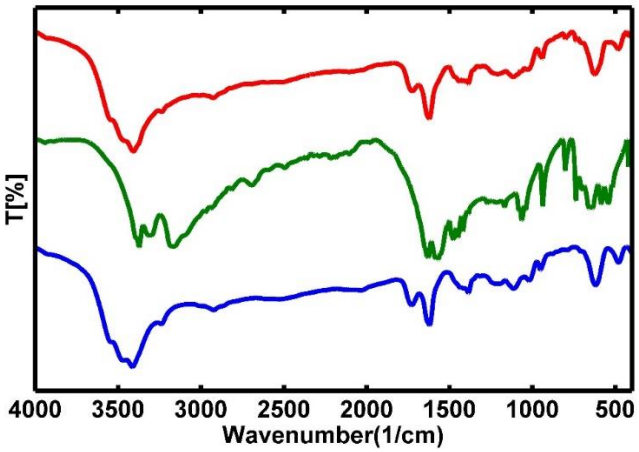

Fig. 1. FTIR spectrum of dendrimer (blue), dendrimer-Cu (green) and dendrimer-Cu-metformin (red).

Statistical Data Analysis

Statistical data analysis was performed using Prism 5 and Microsoft Office 2013, particularly Excel. The data were analyzed using one-way ANOVA, a statistical method for comparing means, followed by Tukey's test, a post-hoc analysis to identify significant differences between groups. A p-value of less than 0.05 was considered statistically significant.

RESULTS AND DISCUSSION

The surface functional groups of the synthesized particles were analyzed using Fourier Transform Infrared Spectroscopy (FTIR) (Figure 1). Peaks observed at 3360 cm^{-1}, 2950 cm^{-1}, 1760 cm^{-1}, 1440 cm^{-1}, and 1240 cm^{-1} correspond to hydroxyl (-OH), alkyl (-CH), carbonyl (-C=O), carboxylic acid (-OH_acid), and ether (C-O) functional groups, respectively. The interaction between copper and the substance reduced the intensity of peaks associated with hydroxyl and acid functional groups. The binding of metformin to the nanoparticle structure led to the appearance of amine peaks at 3401 cm^{-1}, 3337 cm^{-1}, and 2355 cm^{-1}, indicating the presence of the C=N functional group and confirming the successful synthesis of the molecule.

Dynamic Light Scattering (DLS) was used to measure the particle size distribution by analyzing their random movement in a liquid medium (Figure 2). The hydrodynamic diameter of second-generation anionic dendrimer nanoparticles was determined to be approximately 26 nm, with a negative charge of -22.9 mV. The addition of copper increased the hydrodynamic diameter of the Cu-complex to 90 nm. Further, binding metformin to the nanoparticle increased the size to 95 nm and raised the surface charge to +3 mV. The modified Kaiser test indicated that the $–NH_2$ surface loading is approximately 0.65 mmol g^{-1}. Thermogravimetric analysis (TGA) of the synthesized material showed three significant weight losses between 25 and 700 °C. The initial weight loss between 25 and 100°C corresponds to water and physically adsorbed solvents. The second weight loss between 100 and 400°C is likely associated with the dendrimer, while the third is attributed to Cu NPs (Figure S1).

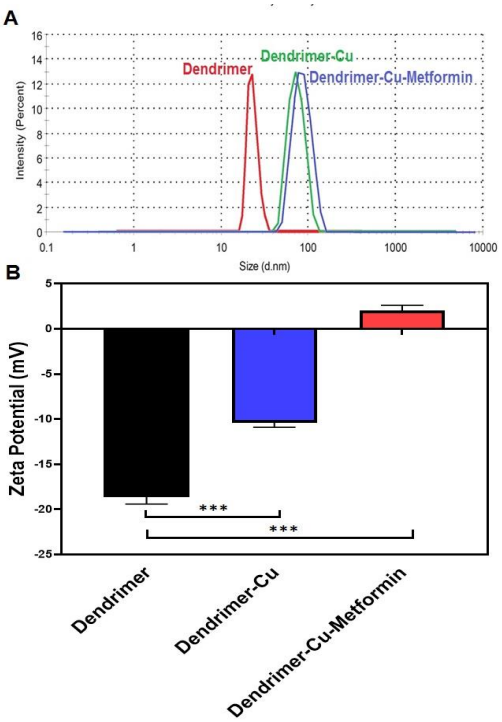

Fig. 2. Size distributions of dendrimer (red), dendrimer–Cu (green) and dendrimer–Cu–metformin (blue) using DLS. Zeta potentials of dendrimer (black), dendrimer–Cu (blue) and dendrimer–Cu–metformin (red)

Corrected Proof

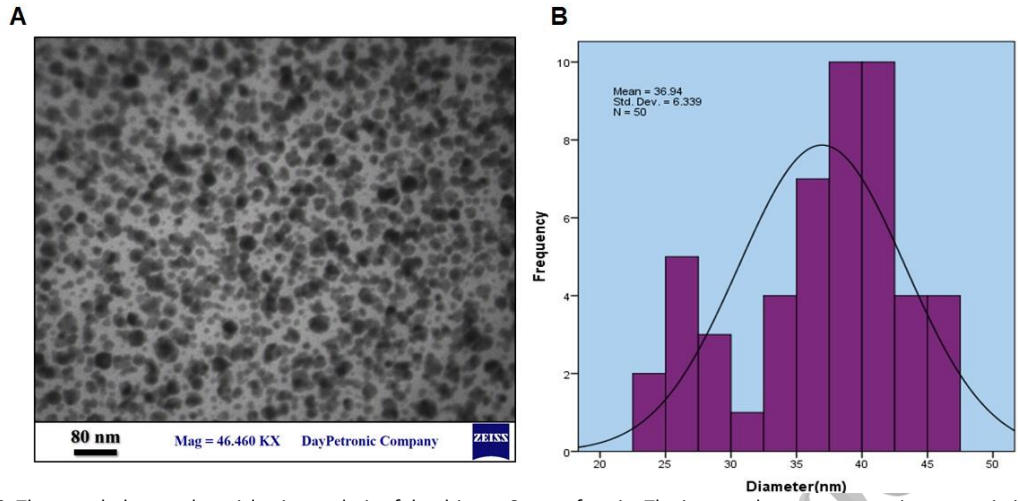

Fig. 3. The morphology and particle-size analysis of dendrimer–Cu–metformin. The images show representative transmission electron microscopy (TEM) images. TEM images used to obtain particle-size distribution (B)

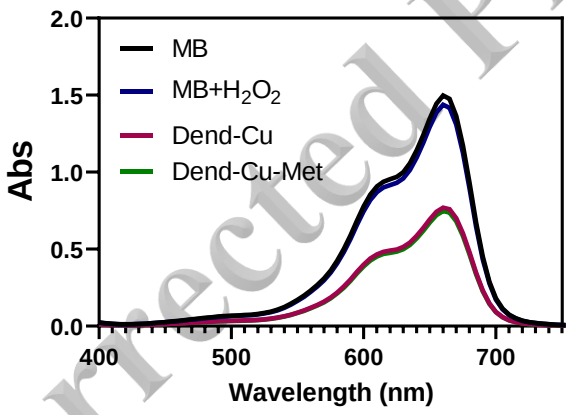

Fig. 4. Degradation spectra of methylene blue: MB (black); MB + H_2O_2 (blue); Dendrimer – Cu (red); and Dendrimer – Cu – metformin (green)

Corrected Proof

Figure 3 displays the results of Transmission Electron Microscopy (TEM) analysis of the size and morphology of the nanoprobe before and after conjugation. TEM analysis revealed spherical particles in various sizes, with an average diameter of 36.94 ± 6.33 nm. The oxidation state of the copper nanoparticles' surface was analyzed using X-ray photoelectron spectroscopy (XPS). Figure S2 shows Cu 2p, O 1s, and N 1s spectra. The initial peak of Cu $2p_{3}/_{2}$, attributed to Cu (II) at a binding energy of 933 eV, corresponds to the CuO species. The satellite peak, at a difference of 8 eV, is assigned to 941.74 eV. The characteristic peak of Cu $2p_{1}/_{2}$ for CuO at 952 eV and its satellite peak at 960 eV, exhibiting an 8 eV difference, can be provisionally assigned [19,20]. A peak at 529 eV in the O 1s spectrum corresponds to O^{2-}, confirming the exclusive presence of CuO species [21]. The 399.7 eV and 399.4 eV peaks correspond to amide and amine groups, respectively [22]. An analysis using MAP confirmed the presence of carbon, oxygen, copper, and nitrogen components (Figure S3).

Methylene blue (MB) was used as an indicator to identify reactive oxygen species (ROS) and detect the subsequent generation of hydroxyl radicals (•OH)[23-25]. The results show that MB degradation occurred only in the presence of both the nanoprobe and H_2O_2 as reactants (Figure 4).

An extensive investigation was conducted to assess the impact of various factors on optimizing labeling efficiency. Using response surface methodology, a central composite design was employed to investigate all variables. According to the information presented in Table 1, the evaluated variables were Labeling Time (C), Reducing Agent (B), and Probe (A), each examined at three distinct levels. For the design, ligand quantities ranged from 10 to 30 mg, the reducing agent varied from 2 to 10 mg, and the period ranged from 5 to 25 minutes. This approach, supported by an appropriate mathematical model, describes the responses. All detailed information and results from the twenty experiments conducted are provided in Table 2.

Table 1. Coding Factor of experimental design

Factor	Name	Unit	-1.68	-1	0	1	1.68
A	Probe	mg	10	15	20	25	30
B	Reduced agent	mg	2	4	6	8	10
C	Time	min	5	10	15	20	25

Table 2. Experimental design result

Resp	Time	Reduced Agent	Probe	RunOrder	StdOrder
21.83	-1.00	1.00	-1.00	1	18
89.42	0.00	0.00	0.00	2	11
96.93	0.00	0.00	1.68	3	13
89.39	0.00	0.00	0.00	4	3
25.65	0.00	1.68	0.00	5	10
38.06	-1.00	-1.00	-1.00	6	16
30.25	1.00	0.00	0.00	7	6
92.04	0.00	0.00	0.00	8	4
66.19	1.00	1.00	1.00	9	7
20.16	1.00	-1.00	-1.00	10	8
64.79	1.00	1.00	-1.00	11	15
35.13	-1.00	-1.00	1.00	12	5
19.19	0.00	-1.68	0.00	13	9
13.32	-1.68	0.00	0.00	14	19
23.90	1.00	-1.00	1.00	15	2
25.86	-1.00	1.00	1.00	16	20
85.60	0.00	0.00	-1.68	17	12
90.38	0.00	0.00	0.00	18	1
91.94	0.00	0.00	0.00	19	17
91.18	0.00	0.00	0.00	20	14

The modeling approach included three parameters: two interaction terms, which account for interactions between the primary components; quadratic terms, which reflect non-linear relationships with the response variable for each primary factor; and three parameters. A comprehensive investigation was conducted using analysis of variance, with the results presented in Table 3. The analysis employed a quadratic mathematical model. The statistical significance of each term is indicated by the P-values obtained during the modeling phase, all of which were less than 0.05. Based on the findings, it was determined that the reducing agent, the square of time, and the interaction between the reducing agent and time all had statistically significant effects. Positive coefficients indicate a direct correlation between the parameter and the response, whereas negative coefficients indicate an inverse correlation. The value of the coefficient reflects the extent to which the parameter impacts the process. According to the study's findings, there is a direct and significant relationship between the increase in each factor and the improvement in labeling efficiency. For a two-dimensional perspective, refer to the diagram below. The correlation between time and the reducing agent significantly affects labeling efficiency, with the most efficient outcomes observed in intermediate time ranges. These findings have been supported by previous research (Figure 5). The sample showed optimal labeling efficiency at 30 mg; however, the reduced agent and shorter duration resulted in efficiencies of 7 mg and 22 minutes, respectively. The sample demonstrated the highest labeling efficiency.

Corrected Proof

Table 3. Analysis of variance result

Term	Coef	SE Coef	T-Value	P-Value
Constant	4.4494	0.0793	56.11	0.000
Probe	0.0359	0.0542	0.66	0.523
Reduced Agent	0.1327	0.0542	2.45	0.034
Time	0.0669	0.0613	1.09	0.301
Probe*Probe	0.0550	0.0526	1.05	0.320
Reduced Agent*Reduced Agent	-0.4454	0.0526	-8.47	0.000
Time*Time	-0.6151	0.0666	-9.24	0.000
Probe*Reduced Agent	0.0126	0.0707	0.18	0.862
Probe*Time	0.0128	0.0707	0.18	0.860
Reduced Agent*Time	0.3810	0.0707	5.39	0.000

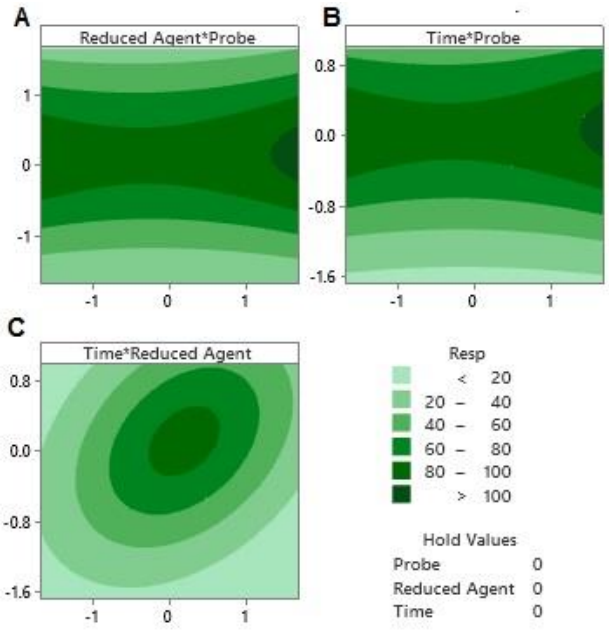

Fig. 5. Response-surface contour plots of the interactions between the amount of reducing agent in the reaction mixture and the amount of probe (A), labeling time and the amount of the probe (B), and labeling time and the amount of reducing agent (C)

Cell culture is essential for developing new medications, as it allows the analysis of specific molecules, natural compounds, or drugs to evaluate their toxicity. Determining the number of viable cells in culture is crucial for understanding a drug's effect. The MTT assay is commonly used in cellular laboratories to assess cell viability by measuring metabolic activity, reflecting the cells' survival ability. The research revealed that at concentrations of 100 µg/mL or lower, nearly 60% of the cells were eradicated. Additionally, the incorporation of metformin enhanced the efficacy of the nanosystem, demonstrating a significant improvement compared to the copper dendrimer group. The dendrimer alone showed no change in activity, as depicted in Figure 6.

Figure 7 displays the results of apoptosis induction using the FITC-V Annexin kit via flow cytometry. Although the experiments were performed three times, only one replicate is shown in the figure. The flow cytometry data indicate that the copper-dendrimer group has a cell viability rate of 60%. The percentages of cells undergoing early and late apoptosis were 12.79% and 20.35%, respectively. Additionally, a small proportion (6.34%) of cells experienced necrosis, likely due to the collection and preparation methods. Introducing metformin into the system reduced the cell survival rate by 6%, increased early apoptosis, and decreased late apoptosis by 20.91% and 14.20%, respectively. Furthermore, an increase in necrosis was observed.

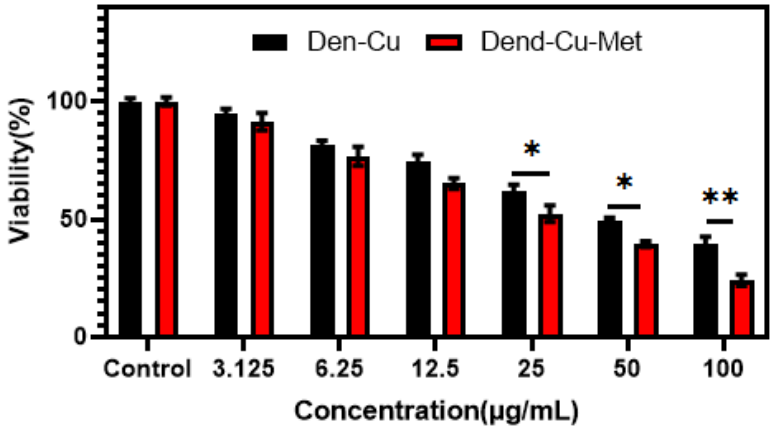

Fig. 6. MTT cell-viability assay of dendrimer–Cu (black) and dendrimer–Cu–metformin (red) at the given concentrations (µg/mL).

Corrected Proof

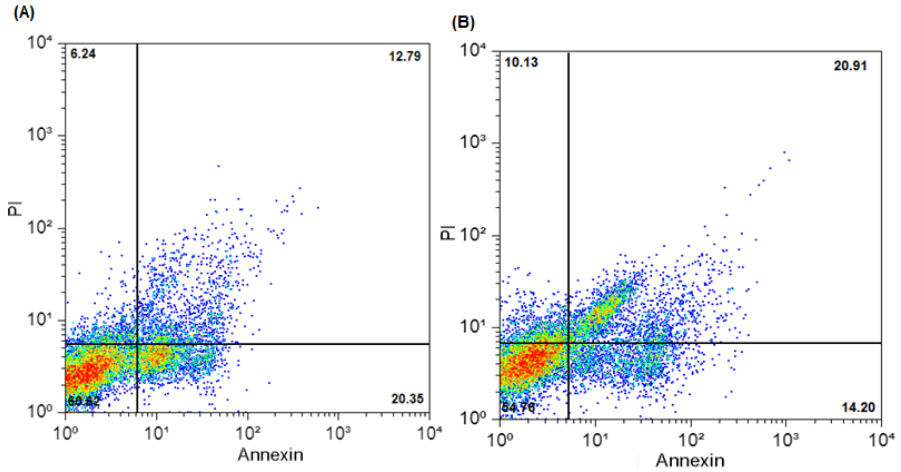

Fig. 7. Dendrimer–Cu and dendrimer–Cu–metformin treated 4T1 cells were examined by Annexin V-FITC/propidium iodide flow-cytometry analysis.

The following are the results of imaging and biodistribution analysis. Upon examination, it was observed that the accumulation in the kidneys increased after 90 minutes. However, the substance buildup in the cancer group decreased and was instead observed in the tumor (Figure 8).

When analyzing the distribution of particles across multiple organs, a significant difference was found between the blocking and tumor groups, particularly in the tumor group. This finding suggests that the particles can selectively target malignancies (Figure 9).

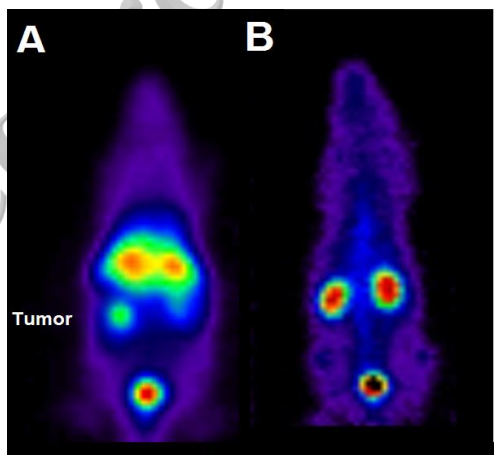

Fig. 8. Tumor-bearing mouse (A) and non-tumor-bearing mouse (B) represented in the form of REW images.

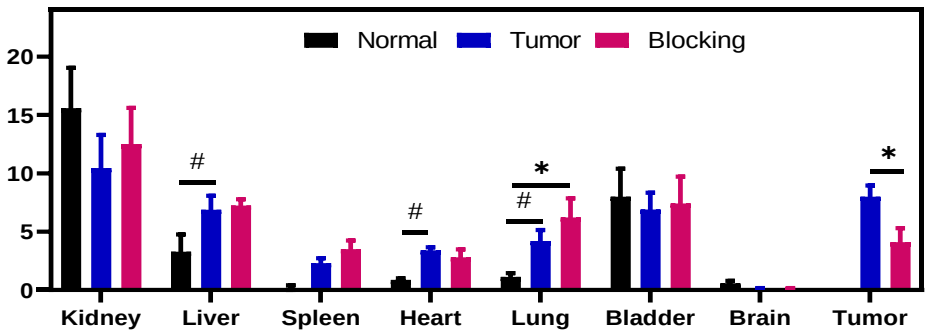

Fig. 9. Radiolabelled nanocomplexes in normal, blocking and tumour-bearing groups, biodistribution of the nanocomplex to the organs.

CONCLUSION

In summary, we have developed an innovative theranostic nanozyme by combining metformin, copper, and dendrimers. This nanozyme has been conjugated with 99mTc using a chelator-free approach. This technology can be applied to both SPECT imaging and cancer treatment. The nanoconjugate offers significant advantages over conventional imaging agents, including rapid tumor dispersion, high efficacy in binding radioactive labels, and swift elimination via the renal system. Biodistribution studies revealed a substantial concentration of the nanoprobe in tumor tissue. Overall, this theranostic approach holds great promise for biomedical applications and offers enhanced imaging capabilities for early cancer detection.

ACKNOWLEDGMENTS

None.

CONFLICT OF INTEREST

The authors have no competing interests.

FUNDING

This is an unfunded research.

ETHICAL CONSIDERATIONS

All experiments with animals were carried out following the recommendations of Tehran University of Medical Sciences, Animal Care and Use Committee (Materials and Methods section).

AUTHOR CONTRIBUTIONS

K. E.: Investigation, writing – original draft preparation, synthesis and characterization of nanoparticles and data collection. **F. Kh.:** Investigation, cellular assays, data collection and formal analysis. **S. A.:** Methodology (development of the dendrimer formulation and synthesis methodology), writing – review and editing. **M. S.:** Characterization, formal analysis and investigation of nanoparticles. **S. E. S. E.:** Methodology, chemical synthesis and conjugation and data interpretation. **M. Sh. A.:** Conceptualization, supervision, project administration, and writing – review and editing. The statements of authors have been approved by all.

AI STATEMENT

This study design and execution, as well as the collection of research data, generation of research data, analysis and interpretation of data, were not carried out by any artificial intelligence (AI) tools.

REFERENCES

1. Ye F, Dewanjee S, Li Y, Jha NK, Chen ZS, Kumar A, et al. Advancements in clinical aspects of targeted therapy and immunotherapy in breast cancer. Mol Cancer. 2023;22(1):105.
2. Ashrafizadeh M, Zarrabi A, Bigham A, Taheriazam A, Saghari Y, Mirzaei S, et al. (Nano) platforms in breast cancer therapy: Drug/gene delivery, advanced nanocarriers and immunotherapy. Med Res Rev. 2023;43.
3. Ye F, Dewanjee S, Li Y, Jha NK, Chen ZS, Kumar A, et al. Advancements in clinical aspects of targeted therapy and immunotherapy in breast cancer. Mol Cancer. 2023;22(1):105.
4. Nolan E, Lindeman GJ, Visvader JE. Deciphering breast cancer: From biology to the clinic. Cell. 2023;186.
5. Munnink TO, Nagengast WB, Brouwers AH, Schröder CP, Hospers GA, Lub-de Hooge MN, et al. Molecular imaging of breast cancer. Breast. 2009;18 Suppl 1:S66–S73.
6. Iranmakani S, Mortezazadeh T, Sajadian F, Ghaziani MF, Ghafari A, Khezerloo D, et al. A review of various modalities in breast imaging: Technical aspects and clinical outcomes. Egypt J Radiol Nucl Med. 2020;51(1):1–22.
7. Na SP, Houserková D. The role of various modalities in breast imaging. Biomed Pap Med Fac Univ Palacky Olomouc Czech Repub. 2007;151(2):209–218.
8. Sree SV, Ng EY, Acharya RU, Faust O. Breast imaging: A survey. World J Clin Oncol. 2011;2(4):171–184.
9. Patel HN, Patel PM. Dendrimer applications: A review. Int J Pharm Bio Sci. 2013;4(2):454–463.
10. Qiao Z, Shi X. Dendrimer-based molecular imaging contrast agents. Prog Polym Sci. 2015;44:1–27.
11. Li H, Zha S, Li H, Liu H, Wong KL, All AH. Polymeric dendrimers as nanocarrier vectors for neurotheranostics. Small. 2022;18(45):2203629.
12. Ambekar RS, Choudhary M, Kandasubramanian B. Recent advances in dendrimer-based nanoplatform for cancer treatment: A review. Eur Polym J. 2020;126:109546.
13. Wolinsky JB, Grinstaff MW. Therapeutic and diagnostic applications of dendrimers for cancer treatment. Adv Drug Deliv Rev. 2008;60(9):1037–1055.
14. Cai X, Hu J, Xiao J, Cheng Y. Dendrimer and cancer: A patent review (2006–present). Expert Opin Ther Pat. 2013;23(4):515–529.
15. Saluja V, Mishra Y, Mishra V, Giri N, Nayak P. Dendrimers based cancer nanotheranostics: An overview. Int J Pharm. 2021;600:120485.
16. Rowson-Hodel AR, Berg AL, Wald JH, Hatakeyama J, VanderVorst K, Curiel DA, et al. Hexamethylene amiloride engages a novel reactive oxygen species- and lysosome-dependent programmed necrotic mechanism to selectively target breast cancer cells. Cancer Lett. 2016;375(1):62–72.
17. Amith SR, Fliegel L. Na+/H+ exchanger-mediated hydrogen ion extrusion as a carcinogenic signal in triple-negative breast cancer etiopathogenesis and prospects for its inhibition in therapeutics. Semin Cancer Biol. 2017;43:35–41.
18. Cardone RA, Alfarouk KO, Elliott RL, Alqahtani SS, Ahmed SB, Aljarbou AN, et al. The role of sodium

Corrected Proof

hydrogen exchanger 1 in dysregulation of proton dynamics and reprogramming of cancer metabolism as a sequela. Int J Mol Sci. 2019;20(15):3694.
19. Poku LO, Cheng Y, Wang K, Sun X. 23Na-MRI as a noninvasive biomarker for cancer diagnosis and prognosis. J Magn Reson Imaging. 2021;53(4):995–1014
20. Van Oosten M, Schäfer T, Gazendam JA, Ohlsen K, Tsompanidou E, de Goffau MC, et al. Real-time in vivo imaging of invasive- and biomaterial-associated bacterial infections using fluorescently labelled vancomycin. Nat Commun. 2013;4:2584.
21. Saluja V, Mishra Y, Mishra V, Giri N, Nayak P. Dendrimers based cancer nanotheranostics: An overview. Int J Pharm. 2021;600:120485.
22. Ghoreishi SM, Khalaj A, Sabzevari O, Badrzadeh L, Mohammadzadeh P, Mousavi Motlagh SS, et al. Technetium-99m chelator-free radiolabeling of specific glutamine tumor imaging nanoprobe: In vitro and in vivo evaluations. Int J Nanomedicine. 2018;13:4671–4683.
23. Li X, Xiong Z, Xu X, Luo Y, Peng C, Shen M, et al. 99mTc-labeled multifunctional low-generation dendrimer-entrapped gold nanoparticles for targeted SPECT/CT dual-mode imaging of tumors. ACS Appl Mater Interfaces. 2016;8(31):19883–19891.
24. Wong SS, Jameson DM, Wong SS. Chemistry of protein and nucleic acid cross-linking and conjugation. Boca Raton: CRC Press; 2012.
25. Fraser SP, Diss JK, Chioni AM, Mycielska ME, Pan H, Yamaci RF, et al. Voltage-gated sodium channel expression and potentiation of human breast cancer metastasis. Clin Cancer Res. 2005;11(15):5381–5389.

Corrected Proof